

Article

Not peer-reviewed version

Formation of natural Magnesium Silica Hydrate(M-S-H) and Magnesium Alumina Silica Hydrate(M-A-S-H) cement

[Håkon Austrheim](#)*, [Depan Hu](#), Niels H Andersen

Posted Date: 25 December 2023

doi: 10.20944/preprints202312.1879.v1

Keywords: Serpentinization; weathering; CO2 sequestration; Feragen and Leka ultramafic complexes; brucite; natural (M-(A)-S-H) cement; duricrust



Preprints.org is a free multidiscipline platform providing preprint service that is dedicated to making early versions of research outputs permanently available and citable. Preprints posted at Preprints.org appear in Web of Science, Crossref, Google Scholar, Scilit, Europe PMC.

Copyright: This is an open access article distributed under the Creative Commons Attribution License which permits unrestricted use, distribution, and reproduction in any medium, provided the original work is properly cited.

Article

Formation of Natural Magnesium Silica Hydrate(M-S-H) and Magnesium Alumina Silica Hydrate(M-A-S-H) cement

Håkon Austrheim ^{1,*}, Depan Hu ^{2,3,4} and Niels H. Andersen ⁵

¹ Corresponding author, The Njord Center, Department of Geology, University of Oslo, P.O. Box 1048 Blindern, Norway. Mobile phone: 4797671977

² Chengdu University of Technology, Chengdu 610059, China.

³ Geoenvironment Monitoring Station in Chengdu, China

⁴ Observation and Research Station of Chengdu Geological Hazards, Ministry of Natural Resources, Chengdu 610042, China

⁵ Department of Chemistry, University of Oslo, Norway

* Correspondence: h.o.austrheim@geo.uio.no,

Abstract: We report on the occurrence of natural Magnesium Alumina Silicate Hydrate (M-(A)-S-H) cement at Feragen and Leka in eastern and western Trøndelag Norway, respectively. Both occurrences are located in the sub-arctic climate zone and form in glacial till and moraine material deposited on ultramafic rock during the Weichselian glaciation. Weathering of serpentinized peridotite dissolve brucite and result in a relative high pH alkaline fluid that subsequently reacts with the felsic minerals of the till (quartz, plagioclase, K-feldspar) to form a cement consisting of an amorphous material or a mixture of nanocrystalline Mg-rich phyllosilicates, including illite. The presence of plagioclase in the till results in the enrichment of alumina in the cement, i.e., forms M-A-S-H instead of the M-S-H cement. Dissolution of quartz results in numerous etch-pits and negative quartz crystals filled with M-A-S-H cement. Where the quartz dissolution is faster than the cement precipitation, a honeycomb-like texture is formed. Compositionally the cemented till (tillite) contains more MgO and has a higher loss of ignition than the till, suggesting that the cement is formed by a MgO fluid that previously reacted with the peridotite. The M-(A)-S-H cemented till represent a new type of duricrust, coined magsilcrete. The study of natural Mg-cement provides information on peridotites as a Mg-source for Mg-cement and as a feedstock for CO₂ sequestration.

Keywords: Serpentinization; weathering; CO₂ sequestration; Feragen and Leka ultramafic complexes; brucite; natural (M-(A)-S-H) cement; duricrust

1. Introduction

Portland cement production contributes c. 8% of the annual anthropogenic CO₂ release [1], albeit some of the CO₂ is recaptured over time. The technology for producing the magnesium analog by calcination of magnesite (MgCO₃) has been available for a century but is even more energy consuming and as well hampered by a high CO₂ release [2]. The search for a CO₂ neutral or CO₂ consuming cement has been focused on the Mg-system [2,3] and hydrated magnesium carbonate (HMC) and magnesium silica hydrates (M-(A)-S-H) are two promising candidates. The HMC cement consist of the hydrocarbonates – hydromagnesite, nesquehonite, landsfordite, dypingite and artenite. Hydrocarbonate formation are also reported from many ultramafic complexes [4,5] and notably Wilson et al. [6] and Power et al. [7] demonstrate that hydrocarbonate can act as a cement by stabilize mine-tailings. Hydration reaction of magnesium oxide and silica produces magnesium silicate hydrate (M-S-H), which provides binding characteristics like Portland cement binder [8]. The formation of magnesium silicates hydrate has been observed at the interfacial zone of cement-based materials in contact with clays [9] and/or as secondary products from the degradation of cementitious materials by groundwater or seawater [10]. M-S-H cement also form in nature. de Ruiter and Austrheim [11] report tillite cemented by M-S-H and Nisiki et al. [12] describes M-S-H formed on

ultramafic rocks by seepage with high activity of Si. Experimentally the presence of aluminum leads to the formation of M-A-S-H where Al^{3+} can replace Mg^{2+} in the octahedral sites and Si^{4+} in the tetrahedral positions [13]. The performance and properties of M-S-H cement may be improved by adding Al [14]. Natural M-A-S-H cement has to our knowledge not previously been recorded.

Magnesium cement has several advantages over Portland cement, in addition to being CO_2 neutral. It forms at a lower pH than Portland cements and is a promising matrix for storage of nuclear waste [15,16]. According to Bernard [17] binders containing M-S-H also have good mechanical properties, dense microstructure and potentially good resistance to leaching. Thus M-S-H is currently of interest as an environmentally friendly alternative to Portland cement due to its potentially lower carbon footprint [2] and for the encapsulation of nuclear waste [18]. The source of MgO is a limiting factor for a large-scale production of Mg cement [3].

De Ruiter and Austrheim [11] discovered and described natural M-S-H from Feragen where a tillite consisting of clasts of quartz, feldspar and ultramafic material was cemented by a hydrous Mg-silicate cement with the average composition of $\text{Mg}_8\text{Si}_8\text{O}_{20}(\text{OH})_8 \cdot 6\text{H}_2\text{O}$, which is a mixture of nanocrystalline Mg-rich phyllosilicates (e.g. kerolite, stevensite and serpentine). The authors suggested that the cement forms from a reaction of quartz with high pH and Mg-rich fluids, which are the result of the dissolution of brucite from the serpentinized ultramafite. De Ruiter and Austrheim [11] focused on the similarity in structure and composition of the naturally formed Mg-silicate cement and human-made M-S-H (magnesium silicate hydrate) cement [19–21]. De Ruiter et al. [22] elaborated on the reaction between the high pH fluid and quartz and highlighted the importance of deformation to enhance dissolution rates of quartz and documented by TEM work that the quartz at the contact with cement developed a μm thick amorphous zone.

In this paper we give additional information of the Feragen M-S-H cement described by de Ruiter and Austrheim [11] and de Ruiter et al. [22]. In addition, we describe a second occurrence from Leka, Norway, reported in a master thesis by Hu [23], where M-S-H grade into M-A-S-H cement in the presence of plagioclase. Here we add a Raman study of the cement at Leka to show that this, like the Feragen cement is amorphous.

2. Methods

Most back-scattered electron (BSE) images and all determination of mineral and cement composition was performed with a Cameca SX100 electron microprobe at the Institute of Geoscience, University of Oslo. Analyses were carried out with an acceleration voltage of 15kv, a beam current of 10 nA and counting time of 10 s for peak and background. For most of the cement analyzes a defocused beam with a diameter of 5 μm was used to reduce evaporation of volatiles. Standard used were synthetic oxides and natural minerals. Matrix corrections followed procedures described by Pouchou and Pichoir [24]. The amount of H_2O was estimated by subtracting the sum of the analyzed oxides from 100%.

Whole-rock geochemical analyses were performed by Actlabs Laboratories Ltd., using the lithium metaborate/tetraborate fusion ICP whole-rock and the trace element ICP/MS packages. For the lithium metaborate/tetraborate fusion ICP Whole Rock Package for major element analysis, samples were prepared and analyzed in a batch system. Each batch contains a method reagent blank, certified reference material and 17% replicates. Samples are mixed with a flux of lithium metaborate and lithium tetraborate and fused in an induction furnace. The molten melt is immediately poured into a solution of 5% nitric acid containing an internal standard and mixed continuously until completely dissolved (~30 minutes). The samples were run for major oxides and selected trace elements on a combination simultaneous/sequential Thermo Jarrell–Ash ENVIRO II ICP or a Varian Vista 735 ICP. Calibrations were performed using 7 prepared USGS and CANMET certified reference materials. One of the 7 standards is used during the analysis for every group of ten samples (www.actlabs.com). FeO was determined through titration, using a cold acid digestion of ammonium metavanadate, and hydrofluoric acid in an open system. Ferrous ammonium sulphate was added after digestion and potassium dichromate was the titrating agent. Weight fractions of dry CO_2 sample gas were measured by infrared absorption after decomposing 0.2g of sample material in a resistance

furnace in pure environment at 1000 °C, using an ELTRA CW-800 (www.actlab.com). For four samples, it was possible to obtain material from both the yellow and the brown weathering zones, but for one sample, only the yellow zone could be separated.

A Horiba Jobin–Yvon (T64000) Spectrograph in micro-single mode configuration was used for the Raman experiments. A Semrock Razoredge longpass filter served to block the Rayleigh light. The entrance slit-width was set to 100 microns. Combined with a 900 lines pr. mm grating, a spectrograph focal length of 640 mm and a 1024 × 256 open electrode CCD with square pixels of 2.56-micron size, a spectral width of 5.1 cm⁻¹ was achieved. The spectral range from 70 to 1800 cm⁻¹ was measured for every sample.

A Spectra-Physics diode pumped Millennia Pro model SJ12 laser yielding 200mW of power at 532.1 nm was used. The beam was guided through a Pellin-Broca prism followed by a pinhole at 1.5m distance to clean up the laser light. A set of three neutral density (ND) filters together with losses at mirrors and the built-in beamsplitter, was used for damping the power to 1.5mW measured at the sample through an Olympus 100x objective. All Raman spectra were scale calibrated against 4-Acetamidophenol (Paracetamol) before and after the sample measurements. No attempts to control polarization was done.

3. Results

3.1. Geological setting and climatic conditions

The Feragen Ultramafic complex (FUC) is located in east central Norway at an altitude between 700 and 900 m a.s.l. (Figure 1a). The area is among the coldest in Europe and located in the subarctic climate zone with monthly mean temperatures ranging between -25 and + 8 °C. The Leka ophiolite complex (LOC) is located on Leka island, Trøndelag, central Norway (Figure 1b) at a latitude of 65 °N. Leka is also situated in the sub-arctic climate zone with monthly mean temperatures ranging between -1 and +15 °C. Like most parts of Scandinavia, the FUC and LOC was glaciated during the Weichselian. This constrains the maximum age of the weathering and duricrust formation to <10ka. The FUC is exposed over an area of 14km². The FUC consists of partly serpentinized harzburgite and dunite [25]. The FUC was extensively mined for chromite, starting in 1824 and terminated in 1939. The mine tailing and locally the mines shafts are coated with hydrocarbonates (4, 22). The carbonation of the mine tailings starts ca. 10 cm below the surface and is particularly well developed on the down facing side of rock fragments in the tailing [22]. On the surface at both FUC and LOC hydrocarbonates only form under overhangs. This together with below surface carbonation of the mine-tailings suggest that the hydrocarbonates are unstable in direct contact with acid rainwater. The LOC contains all the principal components of an ophiolite including a mantle section dominated by peridotite and a layered crustal sequence with alternating dunite, pyroxenite and locally plagioclase rich (anorthositic) layers [26]. The ultramafic parts are exposed over an area of ca 20 km² and is partly serpentinized [27]. Northeast of the village Solsem, South-west Leka (Figure 1b) a m thick conglomerate outcrop over 100 m² is dominated by local clast from the ultramafite and gabbroic rocks, with minor quartz and k-feldspar. Bøe and Prestvik [28] interpreted the conglomerate at Solsem to be a partly lithified morainic deposited from the glaciation. Hu [23] realized that the cementing material at Solsem was similar to the M-S-H cement described from Feragen, although locally containing Al₂O₃.

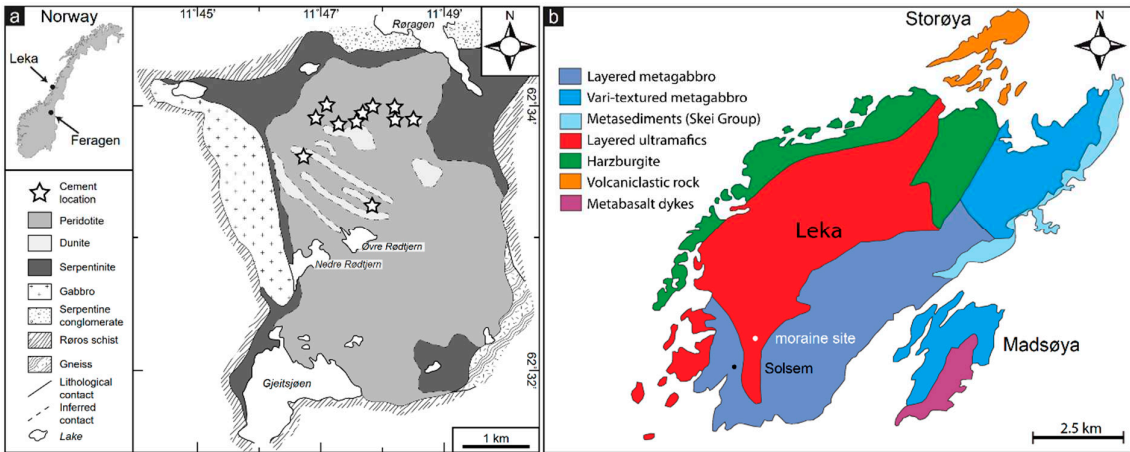


Figure 1. Geological maps of a) the Feragen and b) Leka ultramafic complexes with location of exposed M-(A)-S(H).

3.2. Field and microtextural observations

The weathering of peridotite leaves a few cm thick weathering rind consisting of an outer yellow rim followed inward by blue rim while the unweathered peridotite displays a dark color [29]. The weathering rind is also seen in clasts inside the cemented moraine. Raman mapping has earlier documented that brucite present in the pristine rock was absent in the weathered rims [29]. Microtextural the weathering is evidenced by disappearance and alteration of brucite coupled with a reduction in Mg in weathering zones and an enrichment of Ni and Fe-oxides in aggregates after brucite [30]. Along fault- and fracture- zones, weathering penetrates deep and can be followed downwards for several meters. Hydrocarbonates and pyroaurite form veins in the weathering zone of the clasts and the bedrock. The brucite contains variable amounts of FeO (Table 1) and grades into ferroan brucite.

Table 1. Brucite, Feragen.

SiO2	2,81	0,83	0,16
Al2O3	0,01	0,00	0,01
FeO	15,00	6,28	9,75
MnO	0,62	0,29	0,30
MgO	55,19	61,98	60,10
CaO	0,00	0,07	0,07
Cr2O3	0,01	0,06	0,00
NiO	0,54	0,06	0,60
Total	74,16	69,56	70,95

The cemented till at Feragen is dominated by felsic clasts and is white colored (Figure 2a,b,c) while the cemented moraine at Leka where the amounts of ultramafic material is high display a brownish to greyish color (Figure 2d,e,f). At Feragen, the M-S-H varies in thickness from 0.5 m to cm thick flakes distributed at the surface (Figure 2b). M-S-H is also developed along trenches dug in connection with the mining operation where the fluid could evaporate [11].

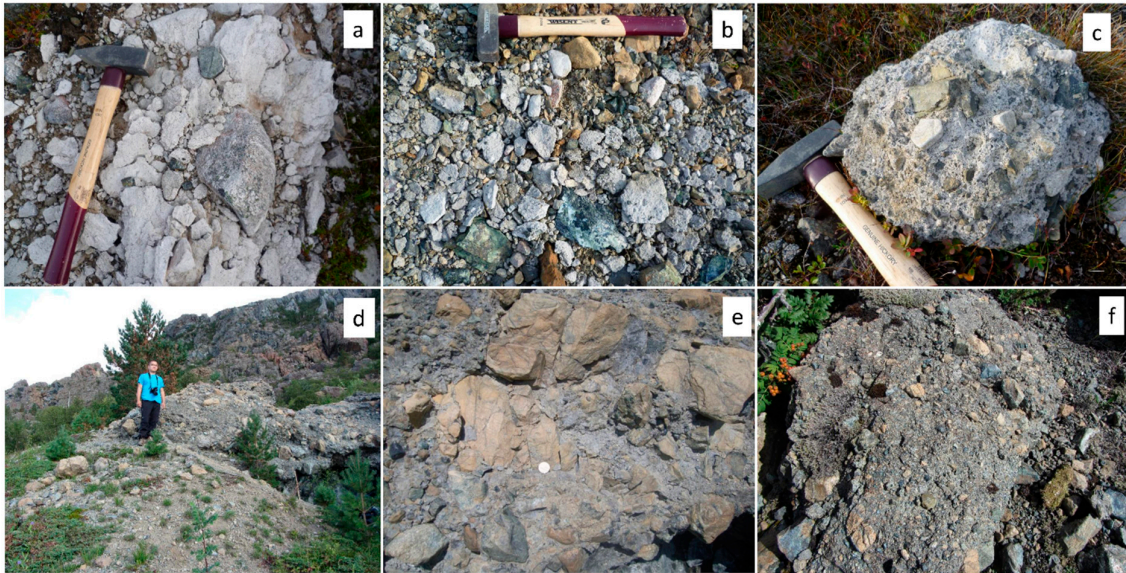


Figure 2. Field photos of M-(A)-S-H cemented till and moraine. a,b,c Feragen and d,e,f Leka. .

The deformed quartz in the till is dissolved and partly replaced by M-S-H cement along sub-grain boundaries (Figure 3a,b,c).

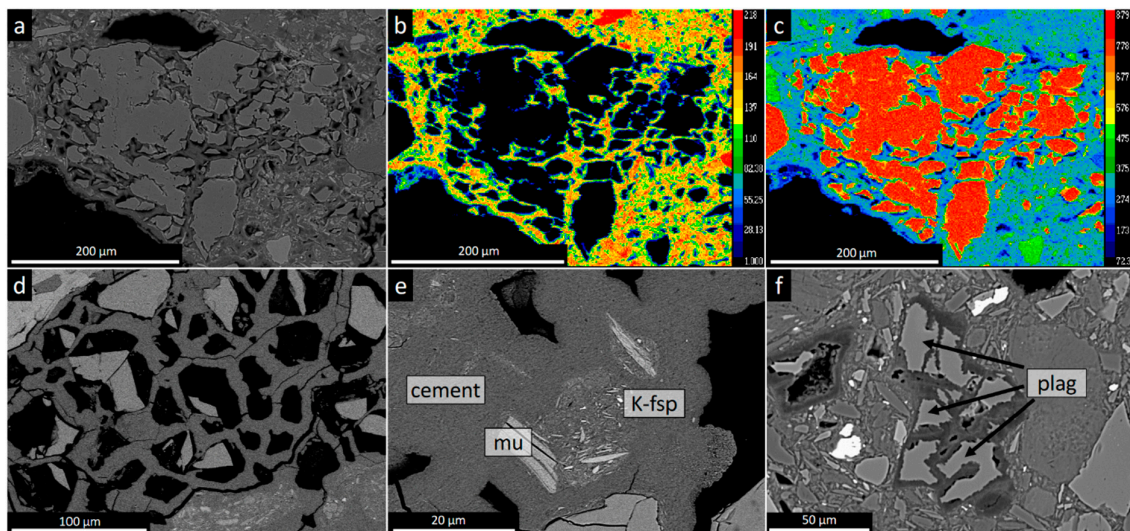


Figure 3. Microtextures of M-(A)-S-H cemented till. a) BSE image showing large quartz grain fragmented by M-S-H cement. b, c) Mg and Si maps of same fragmented grain. d) Honeycomb microtexture after quartz. Some cells contain remnants of partly dissolved quartz. e) M-S-H cement with altered K-feldspar seen as an area of illite rich inclusions. f) Partly dissolved plagioclase (An44), Leka. Veins and fingers of cement penetrate the plagioclase and results in fragmentation and replacement of the grain. Abbreviations: K-fsp: kalifeldspar, mu: muscovite, plag: plagioclase.

Locally the quartz is totally dissolved, and a honeycomb texture is developed (Figure 3d). De Ruiter et al. [22] demonstrated through TEM technique that the dissolution of quartz took place through an amorphous substance. Another characteristic microtexture is etchpits on the surface of the quartz grains. K-feldspar is replaced by and aggregate of cement and μm sized illite (Figure 3e). Locally the aggregates after K-feldspar display flow structures with aligned illite grains. Plagioclase

of varying composition from albite to bytownite (An₈₈) are found as clasts in the cemented till at Leka.

Like quartz, plagioclase is strongly dissolved and partly replaced by cement (Figure 3f; 4a,b,c,d). The cement surrounding the resorbed plagioclase is enriched in Al (Figure 4b). In the same sample, Ca-carbonate surrounds and replace quartz grains (Figure 5a,b), suggesting that Ca released from plagioclase is consumed to form calcite. The M-(A)-S-H cement surrounds and replaces both calcite and quartz (Figure 5a,b).

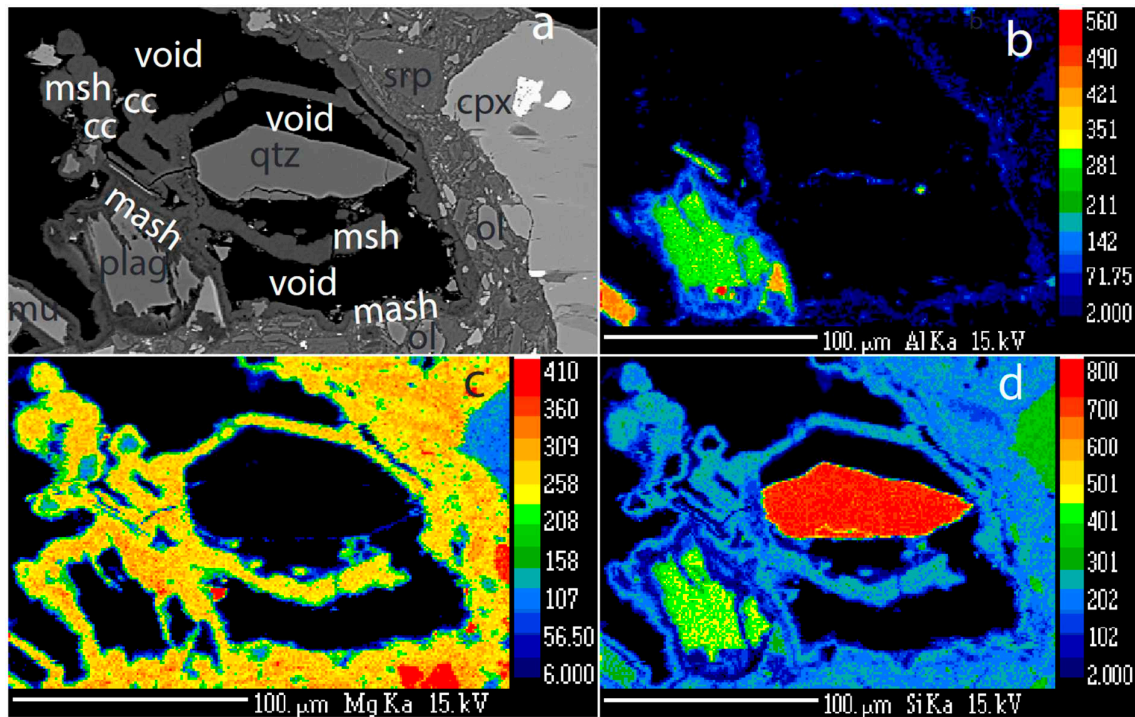


Figure 4. Plagioclase-quartz-cement relationships. a) BSE image of adjacent grains of quartz and plagioclase surrounded by cement. b) Al map over the same area. Note that the Al is present in the cement around the plagioclase and decreases away from the plagioclase grain. c) Si map of the same area. The cement contains lower Si in the Al rich zone adjacent to the plagioclase. d) Mg map of the same area. Notice a thin zone of lower Mg content in the cement adjacent to the relict plagioclase grain. Abbreviations: mash: Al containing cement, plag: plagioclase, mu: muscovite, srp: serpentine, cc: calcite, cpx: clinopyroxene, msh: M-S-H cement, void: empty space.

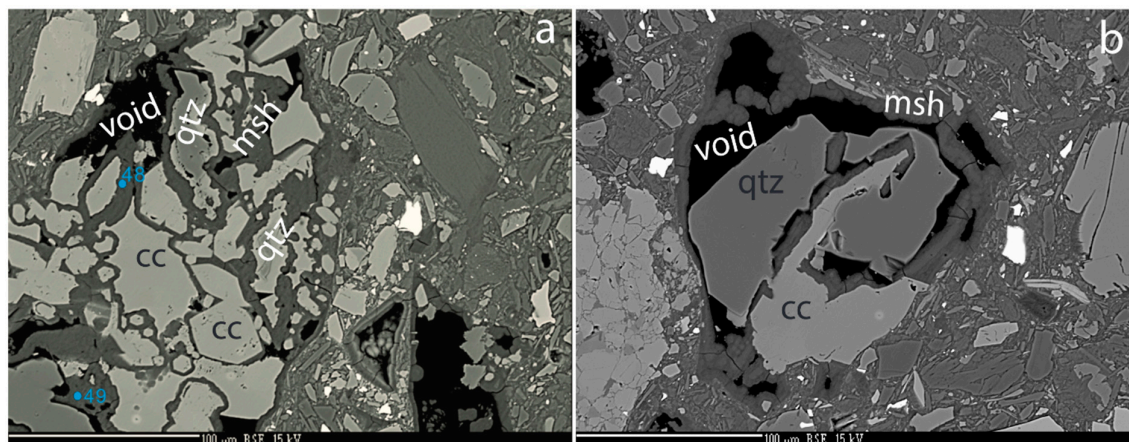


Figure 5. Calcite, quartz, cement relationships. a) BSE image of calcite surrounding quartz grain. Veins of cement penetrated and fragment calcite grains. Abbreviations: qtz: quartz, msh: MSH cement, cc: calcite b) BSE image of calcite vein penetrating and fragmenting quartz grain.

Negative quartz crystals, 50 μm long and veins extending more than 200 μm into quartz grains are filled by cement (Figure 6a,b). The location of spots identified by Raman spectra of the cement, quartz and calcite are shown in Figure 6a,b while their corresponding Raman spectra are shown in Figure 6c. The Raman spectra of the Ca-carbonate give distinct peaks that is characteristic for calcite, but contributions from quartz are visible. The two Raman spectra for the cement are very broad and featureless and no clear peaks could be identified.

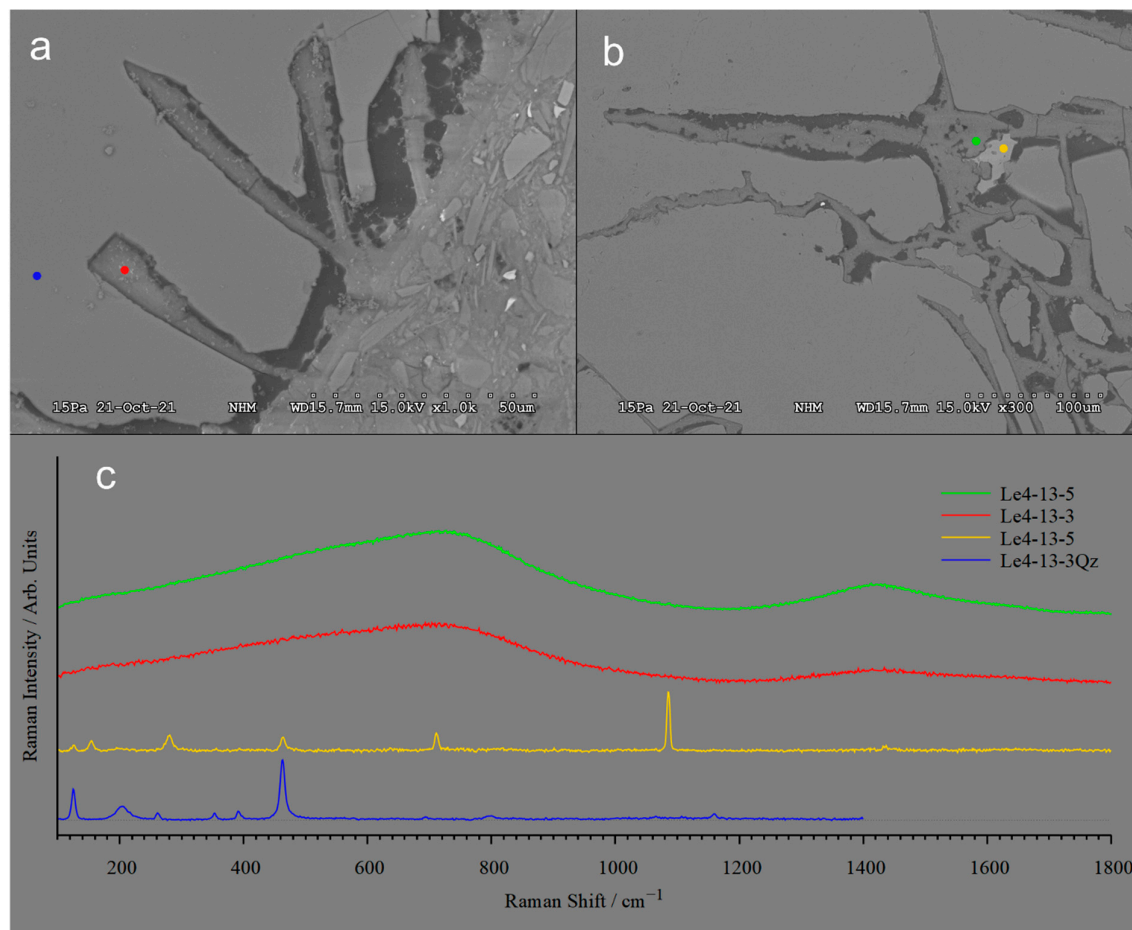


Figure 6. a) Quartz with 50 μm long negative crystals partly filled by M-(A)-S-H cement. b) Veins filled with M-(A)-S-H cement extend > 100 μm into the quartz grain. In the lower right corner, a honeycomb texture has developed. c) Raman spectra of cement filling, dissolved quartz, and carbonate. a) The sharp peaks at 463 and 126 cm^{-1} and the broad peak at 205 cm^{-1} are typical for quartz. b) This spectrum has a peak pattern localized at 154w, 280m, 712m, 1085s and 1435w diagnostic of carbonate as situated in Calcite. In addition to these comes visible residues of the quartz matrix surrounding the Calcite grain. c) & d) Both these Raman spectra are very broad and featureless, and no clear peaks could be identified, typical for an amorphous phase.

3.3. Composition of the cement.

The cement at both Feragen and Leka is dominated by $\text{SiO}_2\text{-MgO-H}_2\text{O}$ (Table 2). Most of the analyses from Feragen contain low Al_2O_3 and cluster in the central part triangular $\text{SiO}_2\text{-MgO-H}_2\text{O}$ diagram while the cement from Leka display more variation (Figure 7a). A high H_2O and low MgO

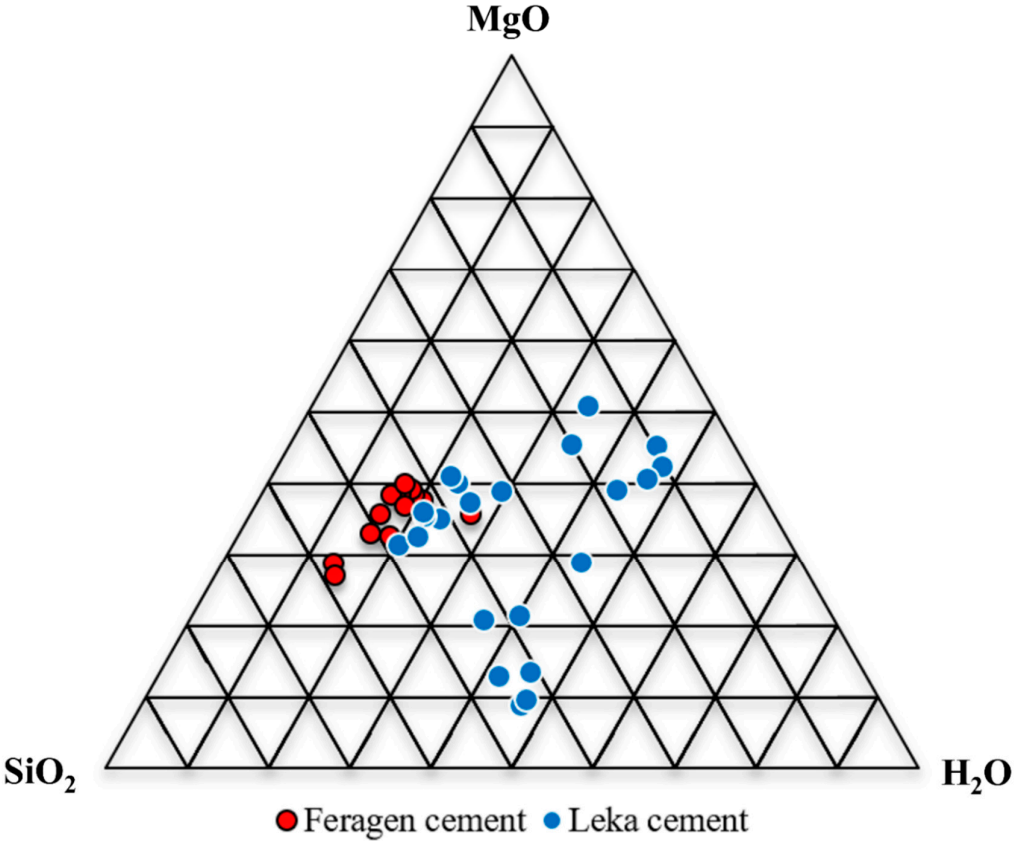
variety is present at Leka (Figure 7a). Analyses from Leka contain high Al₂O₃ (up to 20 wt. %) adjacent to dissolving plagioclase grains. The increase in Al₂O₃ take place on behave of SiO₂ (Figure 7b). The alkalis are low around 0.1 wt. %, but locally concentration up to 2 and 3 wt. % of respectively Na₂O and K₂O is measured.

Table 2. Composition of cement in lithified till and moraine.

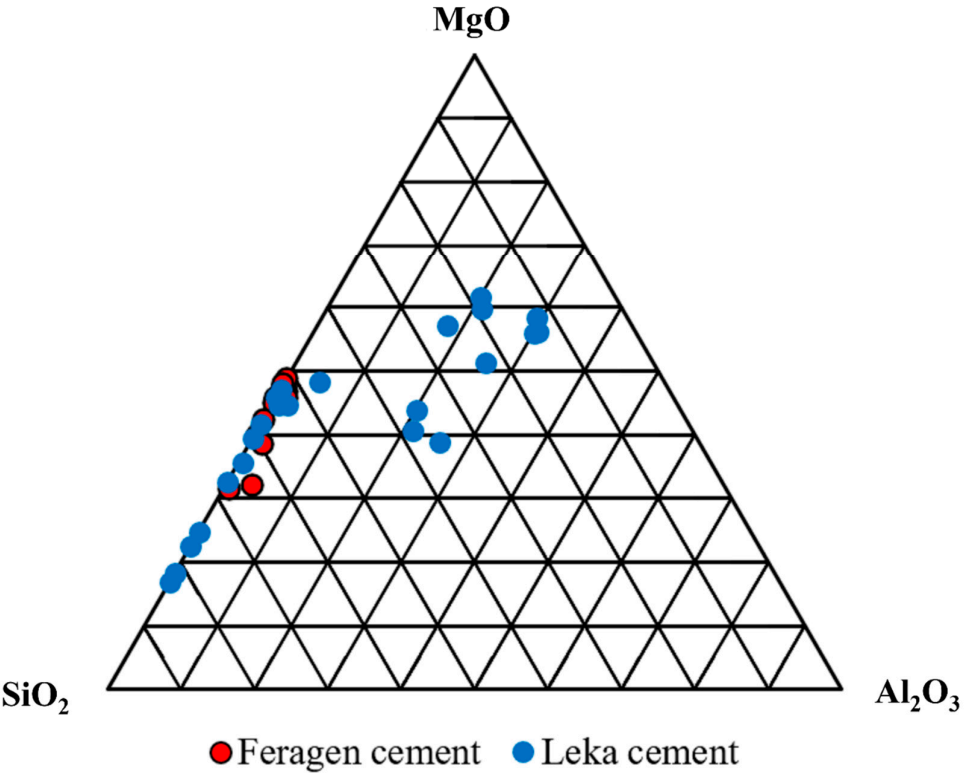
Feragen														
Sample	F9-12	F9-12	F8-12	F8-12	F8-12	F8-12	F8-12	F8-12	F8-12	F8-12	F8-12	F7-12	F7-12	F7-12
SiO ₂	54.75	57.66	42.96	42.09	42.30	42.58	37.24	43.39	45.49	44.55	43.23	48.07	49.61	47.67
TiO ₂	0.05	0.01	0.00	0.00	0.01	0.01	0.00	0.01	0.00	0.00	0.00	0.00	0.00	0.01
Al ₂ O ₃	3.16	0.75	0.18	0.15	0.77	0.36	0.03	1.27	0.01	0.13	0.00	0.39	1.55	0.06
FeO	0.43	0.12	0.15	0.07	0.10	0.13	0.16	0.60	0.06	0.16	0.05	0.29	0.38	0.88
MnO	0.00	0.00	0.05	0.01	0.02	0.02	0.00	0.00	0.00	0.01	0.03	0.09	0.09	0.07
MgO	27.38	26.76	38.95	37.45	37.98	38.81	35.59	37.75	38.37	36.63	39.77	32.19	32.12	35.11
CaO	0.28	0.06	0.07	0.07	0.02	0.01	0.05	0.06	0.10	0.06	0.05	0.23	0.11	0.41
Na ₂ O	0.20	0.00	0.00	0.01	0.00	0.00	0.02	0.06	0.02	0.07	0.01	0.01	0.06	0.08
K ₂ O	0.72	0.03	0.03	0.04	0.13	0.02	0.01	0.29	0.02	0.08	0.01	0.09	0.40	0.02
Cr ₂ O ₃	0.00	0.00	0.00	0.00	0.00	0.04	0.00	0.02	0.00	0.00	0.00	0.05	0.14	0.02
NiO	0.01	0.01	0.07	0.05	0.00	0.06	0.02	0.03	0.00	0.00	0.03	0.08	0.01	0.05
Total	86.97	85.36	82.41	79.89	81.31	82.03	73.03	83.47	84.05	81.63	83.17	81.48	84.25	84.37
H ₂ O	13.03	14.64	17.59	20.11	18.69	17.97	26.97	16.53	15.95	18.37	16.83	18.52	15.75	15.63

Leka														
Sample	L14.1a	L14.1a	L14.1a	L14.1a	L14.1b	L14.1b	L14.1b	L14.1b	L14.1b	L14.1b	L14.1b		L14.1b	L14.1b
SiO ₂	23.04	7.78	8.20	8.45	14.48	44.33	40.95	45.08	43.40	42.94	38.24		26.22	27.47
TiO ₂	0	0.00	0.01	0.00	0.01	0.01	0.00	0	0.00	0.01	0.00		0.01	0.01
Al ₂ O ₃	12.89	18.47	18.68	18.42	16.42	0.02	0.03	0.01	0.03	0.04	0.31		14.75	20.04
FeO	0.73	0.14	0.15	0.36	0.17	0.07	0.04	0.07	0.08	0.07	0.05		0.86	0.17
MnO	0.05	0.00	0.04	0.02	0.06	0.00	0.00	0.00	0.00	0.01	0.09		0.05	0.01
MgO	24.59	36.78	34.42	34.24	32.52	8.94	13.51	13.04	9.68	20.84	21.38		31.96	30.11
CaO	0.73	0.10	0.11	0.04	0.14	0.13	0.14	0.06	0.11	0.17	0.11		1.37	2.82
Na ₂ O	0.14	0.00	0.03	0.00	0.03	0.04	0.02	0.01	0.00	0.01	0.01		0.75	1.96
K ₂ O	0.01	0.00	0.00	0.04	0.28	0.05	0.01	0.06	0.04	0.02	0.05		0.13	0.02
Cr ₂ O ₃	0.04	0.07	0.00	0.00	0.00	0.01	0.01	0.00	0.00	0.00	0.00		0.00	0.02
NiO	0.22	0.15	0.18	0.42	0.00	0.01	0.01	0.00	0.02	0.00	0.02		0.03	0.03
Total	62.44	63.46	61.78	61.88	64.12	53.63	54.67	58.32	53.31	64.09	60.19		76.10	82.65
H ₂ O	37.56	36.54	38.22	38.12	35.88	46.37	45.33	41.68	46.69	35.91	39.81		23.90	17.35

Sample	L14.1b	L14.1b	L14.1b	L14.1b	L14.1b	L14.1b	L14.1b	L14.1b	L14.1b	L14.1b	L14.1b
SiO ₂	11.37	17.45	42.79	13.01	35.13	41.83	33.58	48.01	45.05		
TiO ₂	0.01	0.02	0.00	0.00	0.00	0.01	0.00	0.01	0.01		
Al ₂ O ₃	12.59	12.23	0.75	14.04	3.61	1.70	8.34	0.10	0.31		
FeO	0.16	0.47	0.05	0.13	0.13	0.16	0.64	0.03	0.01		
MnO	0.04	0.05	0.00	0.04	0.01	0.00	0.11	0.00	0.01		
MgO	35.48	39.53	35.18	43.30	36.09	35.20	37.34	31.35	32.47		
CaO	0.00	0.04	0.06	0.23	0.07	0.15	0.08	0.45	0.39		
Na ₂ O	0.05	0.00	0.00	0.35	0.00	0.03	0.01	0.00	0.00		
K ₂ O	0.09	0.02	0.00	0.02	0.03	0.44	0.02	0.02	0.00		
Cr ₂ O ₃	0.00	0.06	0.00	0.01	0.00	0.03	0.05	0.00	0.02		
NiO	0.08	0.09	0.01	0.17	0.09	0.00	0.03	0.01	0.00		
Total	59.85	69.95	78.75	71.31	75.03	79.58	80.20	79.97	78.25		
H ₂ O	40.15	30.05	21.25	28.69	24.97	20.42	19.80	20.03	21.75		



(a)



(b)

Figure 7. a. Composition of cement from Feragen and Leka plotted in triangular ($\text{SiO}_2\text{-MgO-H}_2\text{O}$) diagram (weight %). The samples from Feragen and some of the analysis from Leka cluster in the center of diagram, while the rest of the Leka analysis show a widespread with high H_2O content. b. Same samples plotted in a triangular $\text{SiO}_2\text{-MgO-H}_2\text{O}$ diagram. The samples from Feragen plot along the $\text{SiO}_2\text{-MgO}$ line. The Leka samples contain variable amounts of Al_2O_3 .

3.4. The composition of the weathering rinds

To trace the origin of the elements in the cement we compare weathering rinds of the peridotite with its nonweathered equivalent to test the microtextural indications that peridotite release MgO during weathering. Table 3 lists the compositions for the outer (yellow) and inner (blue) weathering zones compared to the dark pristine peridotite for six samples from Feragen. Also listed in table 1 are two samples of gravel developed locally at the surface of the peridotite. The calculated MgO/SiO_2 , $\text{MgO}/\text{Fe}_2\text{O}_3$, MgO/NiO ratios decreases from the pristine peridotite to the inner blue and outer yellow weathering rinds (Figure 8). This is in accordance with the textural evolution and suggest that MgO leaves the system. The decreasing MgO/NiO ratio in the weathered zones and in the clay gravel fraction (Table 3) suggests that NiO do not follow MgO and remains in the regolith as reported for peridotite regolith in general [31] and for this area [29,30]. The Lanthanide concentration is low (for some of the elements it is below detection limits). There is no obvious systematic change in Lanthanide concentrations and pattern from the unaltered zone to the weathering rinds.

Table 3. Whole rock composition of the blue(inner) and yellow(outer) weathering rinds compared with pristine peridotite(dark) and two samples of gravel.

[illegible]

Ge	0.9	1	0.9	1	1.1	1.1	0.7	0.7	0.8
As	<5	<5	<5	<5	<5	<5	<5	<5	<5
Rb	<1	1	<1	1	1	2	<1	<1	<1
Sr	<2	3	2	<2	<2	<2	<2	<2	<2
Y	<0.5	<0.5	<0.5	<0.5	1.1	0.6	<0.5	<0.5	<0.5
Zr	2	2	<1	3	3	3	<1	<1	<1
Nb	<0.2	<0.2	0.3	<0.2	<0.2	<0.2	<0.2	<0.2	<0.2
Mo	<2	<2	<2	<2	<2	<2	<2	<2	<2
Ag	<0.5	<0.5	<0.5	<0.5	<0.5	<0.5	<0.5	<0.5	<0.5
In	<0.1	<0.1	<0.1	<0.1	<0.1	<0.1	<0.1	<0.1	<0.1
Sn	<1	<1	<1	<1	<1	<1	<1	<1	<1
Sb	0.9	1.2	1.1	0.9	1	0.8	<0.2	<0.2	<0.2
Cs	<0.1	<0.1	<0.1	<0.1	0.1	0.1	<0.1	<0.1	<0.1
Ba	2	7	13	4	4	10	11	<3	<3
La	0.05	0.22	0.17	0.11	0.24	1.19	1.26	0.3	0.07
Ce	0.07	0.21	0.29	0.08	0.16	0.87	2.46	0.44	0.16
Pr	<0.01	0.04	0.04	0.01	0.05	0.14	0.27	0.05	0.02
Nd	<0.05	0.12	0.15	<0.05	0.19	0.55	0.92	0.13	0.06
Sm	<0.01	0.05	0.02	0.05	0.11	0.12	0.1	0.03	0.02
Eu	0.011	0.013	0.011	0.005	0.005	0.015	0.023	0.005	0.005
Gd	<0.01	0.02	0.04	<0.01	0.18	0.04	0.04	0.01	<0.01
Tb	<0.01	<0.01	<0.01	<0.01	0.03	0.01	<0.01	<0.01	<0.01
Dy	<0.01	0.03	0.02	<0.01	0.22	0.1	0.02	<0.01	<0.01
Ho	<0.01	<0.01	<0.01	<0.01	0.04	0.02	<0.01	<0.01	<0.01
Er	<0.01	0.01	0.01	<0.01	0.12	0.05	<0.01	<0.01	<0.01
Tm	0.005	0.005	0.005	0.005	0.016	0.011	0.005	0.005	0.005
Yb	<0.01	0.04	0.02	<0.01	0.08	0.07	<0.01	<0.01	0.01
Lu	0.002	0.006	0.003	0.004	0.011	0.007	0.002	0.002	0.002
Hf	<0.1	<0.1	<0.1	<0.1	<0.1	<0.1	<0.1	<0.1	<0.1
Ta	0.24	0.32	0.29	0.31	0.3	0.38	<0.01	<0.01	0.01
W	1.6	2.6	1.6	3.9	23.8	2.8	<0.5	<0.5	<0.5
Tl	<0.05	<0.05	<0.05	<0.05	<0.05	<0.05	<0.05	<0.05	<0.05
Pb	<5	<5	6	<5	<5	7	<5	<5	<5
Bi	<0.1	<0.1	<0.1	<0.1	<0.1	<0.1	<0.1	<0.1	<0.1
Th	<0.05	<0.05	<0.05	<0.05	<0.05	0.11	0.17	<0.05	<0.05
U	<0.01	0.02	0.02	0.02	0.03	0.07	<0.01	<0.01	<0.01

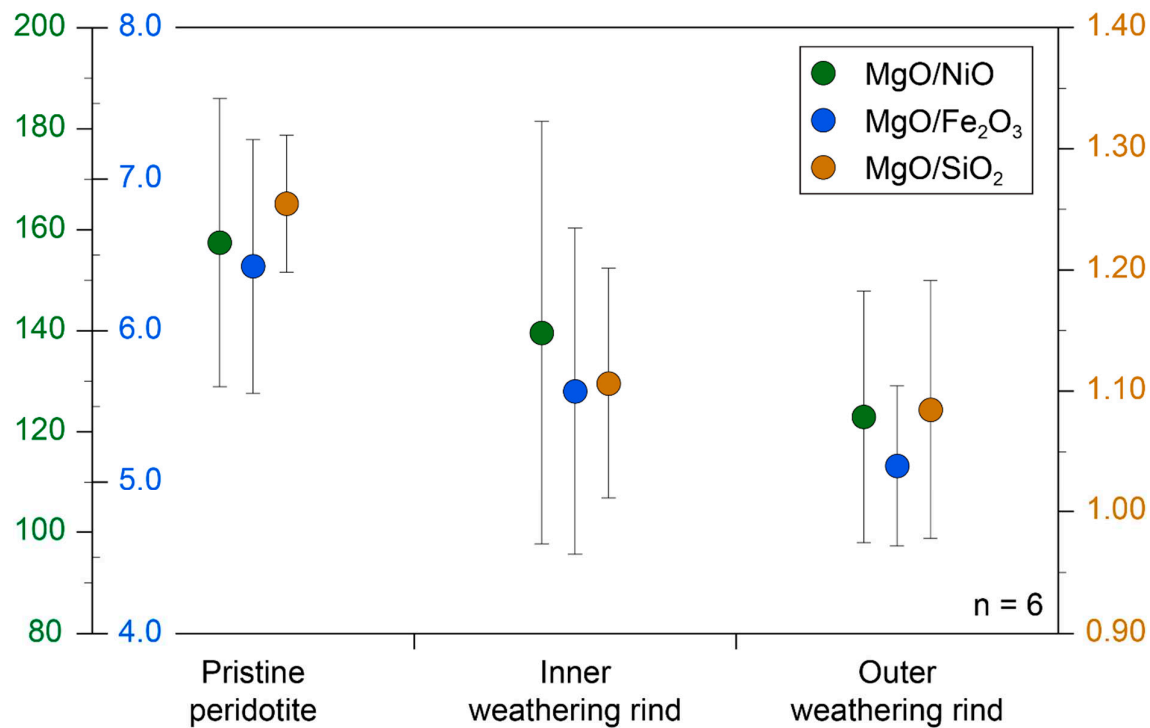


Figure 8. Oxide ratios across the weathering rinds for six samples from Feragen. The error bars denote the 1-sigma standard deviation of the data variability. MgO/NiO, MgO/SiO₂ and MgO/FeO ratios all decreases in the traverse from the pristine peridotite to the intermediate and outer zones. The data is in accordance with a loss of MgO during weathering.

3.5. Composition of till and tillite.

Till is produced by mechanical weathering and is assumed to produce a robust average composition of the upper continental crust [32–35]. Two samples of till from a 40 cm deep trench dug across a mudboil (Figure 9a,b) at Feragen were collected and analyzed for major and trace elements and compared with the nearby tillite (Figure 9c). The two till samples are similar in composition and characterized with elevated SiO₂ and low Al₂O₃ and MgO contents (Table 4). The nearby tillite share the composition of the till for most elements but contain 10 wt. % of MgO and a high LOI content. The chondrite normalized Lanthanide pattern (Figure 10) reveal that the till samples and the cemented till display similar patterns, with a fractionated Light Lanthanides (La/Gd=5.8) and an almost horizontal Intermediate Lanthanides and Heavy Lanthanide segments. The compositions including the Lanthanide patterns suggests that the tillite formed from the till by addition of MgO and H₂O. The Ni concentration in the tillite is low and it appears that the Ni remains in the regolith as is also evident from the textural evolution and the compositions (Table 4).

Table 4. Composition of till from trench through mudboil(FER18/15 and 19/15) and nearby tillite (FER21/15).

	FER18/15	FER19/15	FER21/15
	Trench	Trench	Magcrete
SiO2	87,72	89,58	72,81
Al2O3	4,48	4,23	4,25
Fe2O3(T)	1,54	1,42	1,01
MnO	0,02	0,02	0,01
MgO	0,79	0,63	9,98
CaO	0,26	0,3	0,24
Na2O	0,69	0,7	0,56
K2O	2,11	1,99	1,9
TiO2	0,2	0,21	0,16
P2O5	0,04	0,03	0,03
LOI	0,7	0,52	9,4
Total	98,55	99,61	100,4
Be	< 1	< 1	< 1
V	15	13	12
Cr	110	230	30
Co	4	4	3
Ni	40	40	60
Cu	< 10	< 10	< 10
Zn	< 30	< 30	< 30
Ga	5	4	4
Ge	1	0,8	1,1
As	< 5	< 5	< 5
Rb	53	49	51
Sr	39	45	36
Y	8,7	9,1	9,5
Zr	164	188	136
Nb	4	3,8	4,1
Mo	< 2	4	< 2
Ag	0,7	0,8	0,5
In	< 0.1	< 0.1	< 0.1
Sn	< 1	< 1	< 1
Sb	0,4	0,4	0,5
Cs	0,8	0,7	0,8
Ba	387	376	344
La	11,3	10,1	9,88
Ce	22,6	20,5	19,1
Pr	2,58	2,41	2,3
Nd	9,78	9,01	8,97
Sm	1,98	1,85	1,64
Eu	0,421	0,439	0,432
Gd	1,64	1,56	1,51
Tb	0,27	0,27	0,26
Dy	1,66	1,62	1,54
Ho	0,32	0,33	0,33
Er	0,95	0,97	0,93
Tm	0,147	0,151	0,147
Yb	0,97	1,02	1,02

Lu	0,151	0,159	0,156
Hf	3,5	4,1	3,2
Ta	0,55	0,52	0,53
W	1,5	1,4	1,1
Tl	0,23	0,23	0,22
Pb	7	7	7
Bi	< 0.1	< 0.1	< 0.1
Th	2,66	2,23	1,99
U	0,83	0,85	0,73

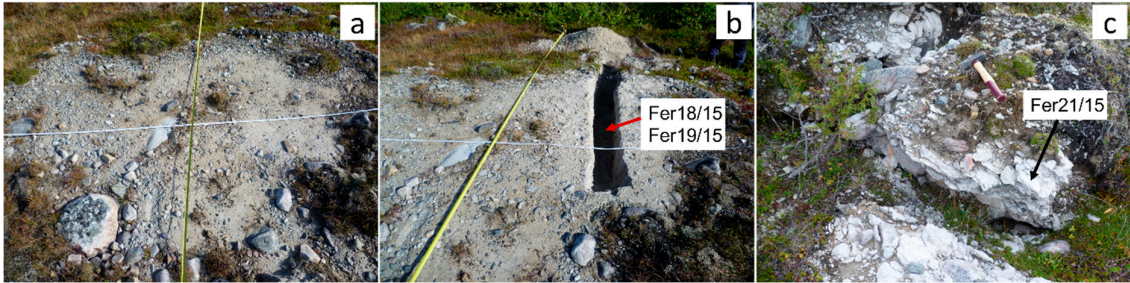


Figure 9. a) Frostboil with till locally covers the ground at Feragen. b) A trench dug through a frostboil reveal a white sand without apparent ultramafic material. c) M-S-H cemented till adjacent to frostboil. A sample (F21-15) from this outcrop was analyzed for major and trace elements and compared with till from the trench (F18-15 and F19-15).

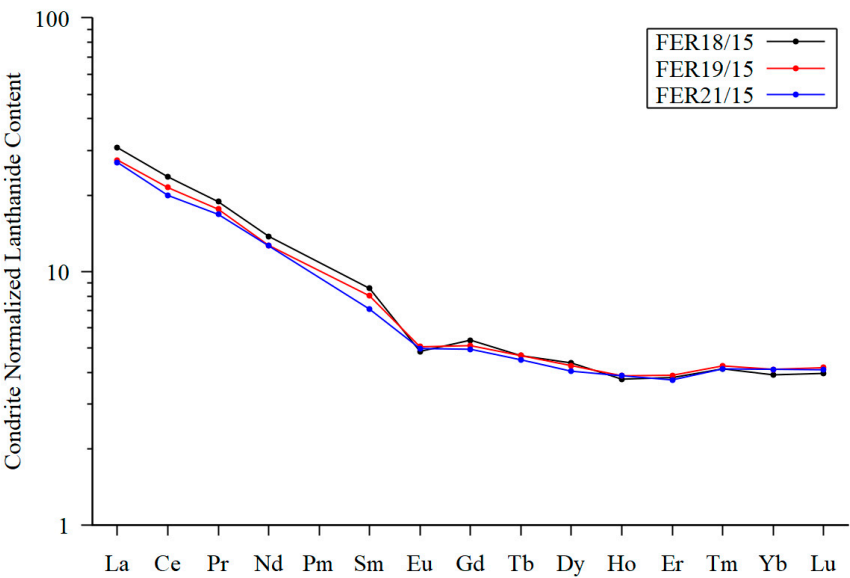


Figure 10. Lanthanide patterns. Chondrite normalized lanthanide pattern for two samples of till (FER18/15 and FER19/15) compared with one sample (FER21/15) from nearby M-S-H cemented till(tillite). Normalization factors are after Taylor and McLennan [55]. The close similarity of the three samples suggests that the tillite has inherited their Lanthanides composition from the till.

4. Discussion

4.1. Formation of natural M-S-H and M-A-S-H cement.

The microtextures and the geochemistry suggest that the Mg present in the cement is derived from the weathering zone of the peridotite by dissolution of brucite. The other natural occurrence of M-S-H cement [11] is also deposited on an ultramafic complex implying that also in that case Mg come from the ultramafic complex. Quartz in contact with M-S-H cement both at Feragen and Leka display dissolution textures (etch pitch and negative crystals filled by M-S-H cement) and in accordance with [10] we interpret that the Si is derived from the felsic material deposited on the ultramafite. We cannot exclude that some Si is derived from dissolved Mg-silicates. However, in the absence of quartz, the Mg fluid form hydrocarbonates and not M-S-H cement. The M-A-S-H is texturally associated with plagioclase and like quartz, plagioclase is dissolved and replaced by cement (Figure 4b). We therefore consider that the M-A-S-H cement obtained its Al from the dissolving plagioclase. The zonation of Al in cement suggest that Al is locally derived. In experimentally formed M-A-S-H cement, Al is added as metakaolin or amorphous Al_2O_3 [13]. The rare occurrence of natural M-S-H cement may reflect the very special geochemical environment where quartz is brought in contact with olivine bearing rocks by glacial activity. Such environment may be restricted to glacial terrains where olivine and quartz are mechanically brought in contact. In magmatic systems olivine and quartz will react at high temperature to form orthopyroxene preventing coexisting olivine in rocks formed by magmatic processes. Glaciers and ice sheets are covering up to 30% of land surface area during glacial cycles [36]. The Snowball Earth Hypothesis suggests that ice entire covered the earth at least twice in its history and the potential for M-S-H formation should be high. Diamictite is present through the geological record on all continent and represent lithified till with a potential for M-S-H formation. Further work will show if the few reports of natural M-S-H cement [11,12] reflects our ignorance of surface processes or if we at Leka and Feragen observe a very rare geological process.

Experimentally produced M-S-H and M-A-S-H cement are produced from amorphous substances in order to speed up reaction rates. Zhang et al. [8] documented that MSH cement can be formed experimentally by reacting brucite and silica-fume. In the natural cases reported here we observe that MSH can form by reacting quartz and a high pH fluid derived by dissolution of brucite. Raman spectra presented for experimentally produced M-S-H cement with varying Mg-Si ratio display peaks suggesting brucite [37,38]. The spectra obtained from the natural occurring cement at Leka (Figure 6c) lack distinct peaks and are typical for an amorphous substance.

4.2. Rate of reaction.

If the cement formed in the time span of 200 years as implied by the presence of M-S-H in the entrance to the Cr-mines which were operating between 1824 and 1939, de Ruiter et al. [22] calculated a dissolution rate for quartz of 1.75×10^{-10} mol $m^{-2}s$, which is 3 order of magnitude faster than the dissolution rate predicted by experimental studies. The microtextures of plagioclase suggest that this mineral also dissolve fast. The selective dissolution and replacement by cement along crystal planes (Figure 6a) and veins (Figure 6b) suggest that experimental determined dissolution rates may not capture the way dissolution and reprecipitation occur in natural rock and that nature provides mechanisms that can greatly enhance dissolution rates. De Ruiter and Austrheim [22] noticed that the quartz from the tillite was strongly deformed as evidenced by undulous extinction and that the cement formed along subgrains. Bacterial activity may also enhance dissolution rates. Ferroan brucite found at both Feragen (Table 1) and Leka [27] may suggest bacterial activity [39]. Whether the identification and cultivating of such mechanisms will speed up the kinetics to satisfy an industrial process, remains an open question.

4.3. The magnesium budgets.

Ultramafic rocks represent a major source of MgO in the form of magnesium silicates. To convert the Mg in silicate to a form that is reactive and applicable in an industrial process is problematic. Gardner and Sui [3] write that there is as yet no known process for making magnesium oxide from natural basic magnesium silicates in an energy-efficient manner, although it may well be possible to invent one given enough support for necessary research. Mg in the form of brucite ($\text{Mg}_x\text{Fe}^{2+}_{(1-x)}(\text{OH})_2$) is a reactive substance [40] that will form MSH cement [41]. The work of Scott et al. [42] demonstrates that brucite ($\text{Mg}(\text{OH})_2$) can be produced from olivine and serpentine through a combination of hydrolysis and acid digestion. To our knowledge this is still not an industrial process. In nature brucite forms from olivine-rich rocks during serpentinization according to the reaction: $\text{Mg}_{1.8}\text{Fe}_2\text{SiO}_4 + \text{H}_2\text{O} = (\text{Mg,Fe})_3\text{Si}_2\text{O}_5(\text{OH})_4 + (\text{Mg,Fe})(\text{OH})_2 + \text{Fe}_3\text{O}_4 + \text{H}_2$. The amount of brucite formed during serpentinization is dependent on a number of parameters such as the rock type being serpentinized, the degree of serpentinization. In addition, the amount of Fe in brucite will increase its amount. We notice that in both at Feragen (Table 1) and Leka [27] the brucite contains high FeO and classifies as Ferroan brucite. The brucite is intergrown with serpentine and difficult to separate mechanically. However, the brucite dissolves in surface water to produce a Mg-containing high pH fluid. This may represent an important way to capture the brucite. Where this fluid comes in contact with the atmosphere it may deposit hydrocarbonates (HMC cement) seen as white coatings under overhangs and in mine-tailings. Beinlich and Austrheim [4] measured the composition of the fluid at Feragen. The pH of mine water ranges from 9.4 to 10.6 with Mg^{2+} and Si (as SiO_2) from 13 to 88.5 mg/L and 0 to 11.5 mg/l respectively. The alkaline water from Leka has a pH up to 10 with Mg and silica in the same range as measured at Feragen [5]. The Mg content of the fluid at Feragen and Leka is one order of magnitude lower than fluid from other similar ultramafics [43,44]. This may mean that the measured fluid had already formed hydrocarbonates. It remains to be tested if the fluid from brucite dissolution can be collected before it deposits hydrocarbonates and if this fluid has advantages as a Mg source over the seawater that contains 52 mmol/l Mg [45].

In nature Mg-silicate can react with CO_2 to form magnesite. Although magnesite is not suitable for producing cement by calcination analog to Portland cement, it is not known if a fluid produced from magnesite will form HMS cement similar to our observation at Feragen and Leka. Possibly the lower pH of such a fluid will prevent the fast dissolution of quartz and plagioclase as described above.

4.4. Serpentinization and weathering

Serpentinization and weathering are used synonymously by some authors, but at Leka and Feragen they are two separated processes. While weathering occurs at and close to the surface, serpentinization occurs at higher temperature ($>200^\circ\text{C}$). As pointed out by Goldich [46] the weathering sequence of igneous rocks is reverse of the Bowen's reaction series meaning that minerals formed at high temperature like olivine weathers faster than rocks formed at lower temperature. Olivine-rich rocks are consequently more strongly weathered than most other rocks. Olivine-rich rocks contain low concentrations of Al_2O_3 (typically between 3 and 0.5%) and cannot form abundant Al-rich phases like kaolinite. Their natural weathering product will be quartz or clay phases consisting of Mg and Si and not necessarily brucite. This is illustrated by [47] who showed that peridotite clast of the Solund basin is altered to dewellite (clay) and quartz. A preconditioning of the peridotite by serpentinization is required to form brucite and weathering is required to dissolve the brucite and form the alkaline fluid.

4.5. The M-(A)-S-H cemented till - a new type of duricrust.

The M-(A)-S-H cemented rock at Feragen and Leka developed within till and moraine at the surface of ultramafic complexes. The M-A-S-H cemented till bears many resemblances to the members of duricrust (calcrete, silcrete). As illustrated in Figure 2 a,d the cemented till appears as cemented gravel. The first use of the term calcrete was indeed referred to as lime-cemented gravel by Lamplugh

[48]. Formation of M-(A)-S-H cemented as a reaction between a precursor sediment and a fluid is a common way of forming duricrust. For example, the calcrete silcrete duricrust at Tswaane were developed within the precursor Kalahari Group sediment by laterally supplied cementing agents [49]. The duricrust formation in the Kalahari case involve reaction between the cementing fluid and the early formed deposited duricrust. The complex relationship between calcite, quartz and M-(A)-S-H cement described above and illustrated in Figure 5a and b suggest that two fluids were involved similar to the duricrust described by Nash et al. [49,50]. Based on the similarities with respect to appearance and formation we interpret the M-(A)-S-H cemented till to represent a new type of duricrust coined magsilcrete. Our knowledge of Martian and planetary crust in general is partly based on testing of crustal analogs [51]. Magsilcrete represent a new analog to be tested towards remote sensing and rover data considering that mafic and ultramafic rocks must be the source material of Martian duricrust [52] where polar glacial ice sheets are present and episodic glaciation took place.

4.6. Formation of natural M(A)SH cement as a geological process

Alteration processes of peridotite (serpentinization, carbonation and weathering) has recently gained increased attention. Serpentinization affect the petrophysical properties of rock and as such influences the geophysical imaging of the lithosphere and its geodynamic evolution. Peridotite (dunite) is the ultimate host rock for in situ CO₂ sequestration. Reaction between olivine and CO₂ according to the reaction $\text{Mg}_2\text{SiO}_4 + \text{CO}_2 = 2\text{MgCO}_3 + \text{SiO}_2$ form 2 mol of magnesite and 1 mole quartz and produces a rock referred to as listvenite. Weathering of peridotite or its alteration product control the Mg-cycle. Mg is a highly mobile element during weathering and preferentially leached out of the crust compared with Si, because Si-rich minerals (alkali feldspar and quartz) are more resistant to chemical and physical weathering than mafic minerals [53].

The formation of magsilcrete as an alteration process of peridotite has up to now not been considered neither as an Mg-reservoir during Mg-cycle modelling nor during modelling of peridotite as feedstock for CO₂ sequestration. As Mg is consumed during magsilcrete formation, less Mg is available for Mg-carbonates. The Mg runoff from the crust is also influence by formation of magsilcrete. Mg isotopes are applied to monitor Mg-cycle. Riverine and ocean waters are enriched in ²⁴Mg compared to the chondritic Mg isotopic composition of the Earth's mantle (Beinlich et al. 54). Beinlich et al. [54] relates this to formation of carbonates (magnesite and dolomite) enriched in ²⁴Mg and the strong weathering of these phase. As magsilcrete forms at low temperatures in equilibrium with hydromagnesite, nesquehonite, landsfordite, artemite and dypingite it is also likely that it fractionates Mg-isotope. It remains to be determined how this low temperature alteration (weathering) fractionates Mg isotope and thus change the foundation for modelling the Mg-cycle.

5. Conclusions

The natural process of forming M-(A)-S-H cement involve two steps - formation of brucite by serpentinization of peridotite and subsequent dissolution of brucite during weathering to form a reactive Mg rich high pH fluid. The alkaline fluid dissolve quartz and precipitate M-S-H cement. Where plagioclase is present in the reacting material Al enters the cement and forms M-A-S-H cement. Both M-S-H and M-A-S-H is formed in glaciated area where glaciation deposited quartz and feldspar on to surface of ultramafic complexes. The cemented till and moraine belong to the family of duricrusts and represent a new type of duricrust that we call magsilcrete.

Author Contributions: Conceptualization, Håkon Austrheim; Investigation, Depan Hu; Methodology, Niels Andersen; Visualization, Depan Hu; Writing – original draft, Håkon Austrheim; Writing – review & editing, Niels Andersen.

Funding: The Raman work was cover through the NRF supported project NATSORB.

Institutional review Board Statement: Not applicable.

Informed Consent Statement: Not applicable.

Data Availability Statement: Not applicable.

Acknowledgments: We thank Dag Dysthe, Andreas Beinlich, Lisa de Ruiter and Ole Ivar Ulven for discussion and advice during the progress of this work.

Conflicts of interest: The authors declare that there that there is no conflict of interest regarding the publication of this paper.

References

1. Schrivener, K.L.; John, V.M.; Gartner, E.M. Eco-efficient cement: Potential economically viable solutions for a low-CO₂ cement-based materials industry. *Cem. Concr. Res.*, **2018**, *114*, 2-26.
2. Walling, S.A.; Provis, J.L. Magnesia-based cements: a journey of 150 years, and cements for the future? *Chem. Rev.* **2016**, *116*, 4170-4204.
3. Gartner, E.; Sui, T. Alternative cement clinkers. *Cem. Concr. Res.* **2018**, *114*, 27-39.
4. Beinlich, A.; Austrheim, H. In situ sequestration of atmospheric CO₂ at low temperature and surface cracking of serpentinized peridotite in mine-shafts. *Chem. Geol.* **2012**, *332-333*, 32-44.
5. Økland, I.; Huang, S.; Dahle, H.; Thorseth, I.H.; Pedersen, R.B. Low temperature alteration of serpentinized ultramafic rock and implication for microbial life. *Chemical Geology* **2012** *318-319*, 75-87.
6. Wilson, S.A.; Dipple, G.M.; Power, I.M.; Thom, J.M.; Andersen, R.G.; Raudsepp, M.; Gabites, J.E.; Southam, G. Carbon dioxide fixation within mine wastes of ultramafic-hosted ore deposits: Examples from the Clinton Creek and Cassiar crysotile deposits, Canada. *Economic Geology* **2009**, *104*, 95-112.
7. Power, I.M.; Wilson, S.A.; Dipple, G.M. Serpentine carbonation for CO₂ sequestration. *Elements* **2013**, *9*, 115-121.
8. Zhang, T.; Vandeperre, L. J.; Cheeseman, C. R. Formation of magnesium silicate hydrate (M-S-H) cement pastes using sodium hexametaphosphate. *Cement and Concrete Research* **2014**, *65*, 8-14.
9. Jenni, A.; Mäder, U.; Lerouge, C.; Gaboreau, S.; Schwyn, B. In situ interaction between different concretes and Opalinus clay, *Physics and Chemistry of the Earth, Parts A/B/C*, **2014**, *70*, 71-83. <https://doi.org/10.1016/j.pce.2013.11.004>
10. Mäder, U.; Jenni, A.; Lerouge, C.; Gaboreau, S.; Miyoshi, S.; Kimura, Y.; Cloet, V.; Fukaya, M.; Claret, F.; Otake, T.; Shibata, M.; Lothenbach, B. 5-year chemico-physical evolution of concrete-claystone interfaces, *Swiss J Geosci.* **2017**, *110*, 307-327.
11. de Ruiter, L.; Austrheim, H. Formation of magnesium silicate hydrate cement in nature. *J. Geol. Soc. Lond.* **2018**, *175*, 308-320.
12. Nishiki, Y.; Sato, T.; Katoh, T.; Otake, T.; Kikuchi, R. Precipitation of magnesium silicate hydrates in natural alkaline surface environments. *Clay Science* **2020**, *24*, 1-13.
13. Benard, E.; Lothenbach, B.; Cau-Dit-Coumes, C.; Pochard, I.; Rentsch, D.. Aluminium incorporation into magnesium silicate hydrate (M-S-H) Cement and Concrete Research **2020**, *128*, 105931. <https://doi.org/10.1016/j.cemconres.2019.105931>
14. Benard, E.; Lothenbach, B.; German, A.; Rentsch, D.; Winnefeld, F. Effect of aluminate and carbonate in magnesium silicate cement. *Cem. Concr. Composites* **2023**, *139*, 105010.
15. Mariske, M.R.; Debus, C.; Di Lorenzo, F.; Bernard, E.; Churakov, S.V.; Ruiz-Agudo, C. Immobilization of (Aqueous) Cations in Low pH M-S-H Cement. *Appl. Sci.* **2021**, *11*, 2968. <https://doi.org/10.3390/app11072968>
16. Zhang, T.; Cheeseman, C. R.; Vandeperre, L. J. Development of low pH cement systems forming magnesium silicate hydrate (M-S-H). *Cem. Concr. Res.* **2011**, *41*, 439-442.
17. Bernard, E. Research progress on magnesium silicate hydrate phases and future opportunities. *RILEM Technical Letters* **2022**, *7*, 47-57. <https://doi.org/10.21809/rilemtechlett.2022.162>
18. Zhang, T.; Li, T.; Zou, Y.; Li, S.; Zhi, Y.; Cheeseman, C.R. Immobilization of radionuclide ¹³³Cs by magnesium silicate hydrate cement, *Materials* **2012**, *13*
19. Brew, D.R.M.; Glasser, F.P. Synthesis and characterization of magnesium silicate hydrate gels. *Cem. Concr. Res.* **2005**, *35*, 85-98.
20. Roosz, C.; Grangeon, S.; Blanc, P.; Montoullout, V.; Lothenbach, B.; Henocq, P.; Giffaut, E.; Vieillard, P.; Gaboreau, S. Crystal structure of magnesium silicate hydrates (M-S-H): The relation with 2:1 Mg-Si phyllosilicates. *Cem. Concr. Res.* **2015**, *73* 228-237 <https://doi.org/10.1016/j.cemconre.2015.03.014>
21. Zhang, Y.; Chang, J.; Zhao, J.; Fang, Y. Nanostructural characterization of Al(OH)₃ formed during the hydration of calcium sulfoaluminate cement. *J. Am. Ceram. Soc.* **2018**, *101*, 4262-4274.
22. De Ruiter, L.; Gunnæs, A.E.; Dysthe, D.K.; Austrheim, H. Quartz dissolution associated with magnesium silicate hydrate cement precipitation. *Solid Earth* **2021**, *12*, 389-404.
23. Hu, D. The Characterization of the cementing materials in the ultramafic tillites from Feragen and Leka, Norway. Master Thesis University of Oslo. **2015** pp 124
24. Pouchou, J.L.; Pichoir, F. Quantitative Analysis of Homogeneous or Stratified Microvolumes Applying the Model PAP in Heinrich, K.F.J.; Newbury, D.E. (Eds.) Springer Boston MA, USA, **1991**

25. Moore, A. C.; Hultin I. Petrology, mineralogy, and origin of the Feragen ultramafic body, Sor-Trondelag, Norway. *Norsk Geologisk Tidsskrift*. **1980**, 60, 235–254.
26. Prestvik, T. The Caledonian ophiolite complex of Leka, central Norway. In: Panayiotou, A. (Ed.), *Ophiolites*. Geol. Surv. Dep, Cyprus, **1980**, 555-556.
27. Iyer, K.; Austrheim, H.; John, T.; Jamtveit, B. Serpentinization of the oceanic lithosphere and some geochemical consequences: Constraints from the Leka Ophiolite Complex, Norway. *Geohem. Geol.* **2008**, 249 66-90
28. Bøe, P; Prestvik, T. A serpentinite conglomerate on the Island of Leka, Nord-Trøndelag. *Norsk Geologisk Tidsskrift* **1974**, 54, 117-121.
29. Ulven O. I.; Beinlich A.; Hövelmann J.; Austrheim H.; Jamtveit B. Subarctic physicochemical weathering of serpentinized peridotite. *Earth Planet. Sci. Lett.* **2017**, 468, 11–26.
30. Beinlich, A.; Austrheim, H.; Mavromatis, V.; Grguric, B.; Putnis, C.V.; Putnis, A. Peridotite weathering is the missing ingredient of Earth's continental crust composition. *Nature Com.* **2018**, 9:634.
31. Gleeson, S.A.; Herrington, R.J.; Durango, J.; Velasquez, C.A.; Koll, G. The mineralogy and geochemistry of the Cerro Matoso, S.A. Ni laterite deposit, Montelibano, Colombia. *Econ. Geol.* **2004**, 99, 1197-1213
32. Goldschmidt, V.M. Grundlagen der quantitativen geochemie. *Fortschritte der Mineralogie, Krystallographie und Petrologie* **1933**, 17, p.112.
33. Goldschmidt, V.M. *Geochemistry*. Oxford University Press, Oxford **1958**.
34. Canil, D. and Lacourse, T. An estimate for the bulk composition of juvenile upper continental crust derived from glacial till in the North American Cordillera. *Chem. Geol.* **2011**, 284, 229-239.
35. Gaschnig, R.M.; Rudnik, R.L.; McDonough, W.F.; Kaufman, A.J.; Valley, J.W.; Hu, Z.; Gao, S.; Beck, M.L. Compositional evolution of the upper continental crust through time, as constrained by ancient glacial diamictites. *Geochim. Cosmochim. Acta* **2016**, 186, 316-343
36. Hawkings, J.R.; Wadham, J.L.; Benning, L.G.; Hendry, K.R.; Tranter, M.; Tedstone, A.; Nienow, P.; Raiswell, R. Ice sheets as a missing source of silica to the polar oceans. *Nature Com.* **2017**, 8: 4198.
37. Lothenbach, B.; Nied, D.; L'Hopital, E.; Achiedo, G.; Dauzeres, A. Magnesium and calcium silicate hydrates. *Cement and Concrete Research* **2015** 77, 60-68
38. Nied, D.; Enemark-Rasmussen, K.; L'Hopital, E.; Skibsted, J. Properties of magnesium silicate hydrates(M-S-H) *Cement and Concrete Research* **2015** 79, 323-332. <http://doi.org/10.1016/j.cemconres.2015.10.003>
39. Templeton, A.S.; Ellison, E.T. Formation and loss of metastable brucite: does Fe(II)-bearing brucite support microbial activity in serpentinizing ecosystems? *Philosophical Transactions Royal Society.* **2020** A378:20180423. <http://dx.doi.org/10.101098/rsta.2018.0423>.
40. Hövelmann, J.; Putnis, C.; Ruiz-Agudo, E.; Austrheim, H. Direct Nanoscale Observations of CO₂ Sequestration during Brucite (Mg (OH)₂) dissolution. *Environmental Science & Technology.* **2012**, Dx.doi.org/10.1021/es300403n
41. De Ruiter, L.; Putnis, C.V., Hövelmann, J., King, H.E. and Austrheim, H. Direct Observation of the Coupling between Quartz Dissolution and Mg-Silicate Formation. *ACS Earth and Space Chemistry* **2021**, DOI: 10.1021/acsearthspacechem.8b00197
42. Scott, A.; Oze, C.; Shah, V.; Yang, N.; Shanks, B.; Cheeseman, C.; Marshall, A; Watson, M. Transformation of abundant magnesium silicate minerals for enhanced CO₂ sequestration. *Communications Earth & Environment.* **2021**, 2, 25
43. Barnes, L.; O'Neil, J.R. The relationship between fluids in some fresh alpine-type ultramafics and possible modern serpentinization, Western United States. *Geol. Soc. Am. Bull.* **1969** 80, 1947
44. Boschetti, T.; Toscani, L. Springs and streams of the Taro-Ceno Valleys (Northern Appennini, Italy): reaction path modeling of waters interacting with serpentinized ultramafic rocks. *Chem. Geol.* **2008** 257, 76-91
45. Seeger, M.; Otto, W.; Flick W. Magnesium Compounds. In: *Ullmann's Encyclopedia of Industrial Chemistry*. John Wiley & Sons, Ltd. **2011** <https://doi.org/10.1002/14356007.q15.595.pub2>
46. Goldich, S.S. A study of rock weathering. **1938** *J. of Geol.* 46, 17-58 <https://www.journal.uchicago.edu/doi/abs/10.1086/624619>
47. Beinlich, A.; Austrheim, H.; Glodny, J.; Erambert, M.; Andersen, T.B. CO₂ sequestration and extreme Mg depletion in serpentinised peridotite clasts from the Devonian Solund basin, SW-Norway. *Geochim Cosochim Acta* **2010**, 74:6935-6964.
48. Lamplugh, G.W. Calcrete. *Geological Magazine* **1902**, 9, 575.
49. Nash, D.J.; Shaw, P. Silica and carbonate relationships in silicret-calcrete intergrade duricrusts from the Kalahari of Botswana and Namibia. *J. of African Earth Sciences* **1998**, 27, 11-25
50. Nash, D.J.; McLaren, S.J.; Webb, J.A. Petrology, geochemistry and environmental significance of silicrete-calcrete intergrade duricrust at Kang Pan and Tswaane, Central Kalahari, Botswana. *Earth Surf. Process. Landforms* **2004**, 29, 1559-1586.
51. Lewinger, W.; Comin, F.; Matthews, M.; Saaj, C. 2018. Earth analogue testing and analysis of Martian duricrust properties. *Acta Astronautical* **2018** 152, 567-579.

52. Clark, B.C.; Baird, A.K.; Weldon, R.J.; Tusaki, D.M.; Schnabel, L.; Candelaria, M.P. Chemical composition of Martian fines. *J. Geophys. Res. Solid Earth* **1982** 87, B12, 10059-10067
53. Holland, H.D. *The chemical evolution of the Atmosphere and Ocean*, Princeton University Press, Princeton, NJ. **1984**
54. Beinlich, A.; Mavromatis, V.; Austrheim, H.; Oelkers, E.H. Inter-mineral Mg isotope fractionation during hydrothermal ultramafic rock alteration- Implications for the global Mg-cycle. *Earth and Planet. Sci. Letter* **2014** 392, 166-176
55. Taylor, S.R.; McLennan, S.M. *The Continental Crust: Its Composition and Evolution*. Blackwell, Oxford, 1-312 **1985**

Disclaimer/Publisher's Note: The statements, opinions and data contained in all publications are solely those of the individual author(s) and contributor(s) and not of MDPI and/or the editor(s). MDPI and/or the editor(s) disclaim responsibility for any injury to people or property resulting from any ideas, methods, instructions or products referred to in the content.